Scientific paper

Correlation Between Electronic and Corrosion Properties of the Passive Oxide Film on Nitinol

Jozefina Katić and Mirjana Metikoš-Huković*

Department of Electrochemistry, Faculty of Chemical Engineering and Technology, University of Zagreb, P.O. Box 177, 10000 Zagreb, Croatia

** Corresponding author: E-mail: mmetik@fkit.hr*
Phone: +385 1 4597 140, Fax: +385 1 4597 139

Received: 05-02-2014

Paper based on a presentation at the 4th RSE-SEE 2013 Symposium on Electrochemistry in Ljubljana, Slovenia

Abstract

The oxide film (TiO_2) was formed on Nitinol potentiostatically in an acetic acid solution. Deep understanding of electronic properties of this film is needed to predict long-term corrosion properties of Nitinol implant material in simulated body fluid conditions. The capacitance measurements were performed under depletion conditions to study electronic (semiconducting) properties. The space charge, formed at the solid|liquid interface, creates the barrier for the corrosion processes in aggressive (bio)environment. According to the results of electrochemical impedance spectroscopy (EIS) and Mott-Schottky analysis (MS), the passive film on Nitinol behaves as amorphous highly-doped n-type semiconductor. The values of electronic structure parameters (the flat-band potential, E_{fb} and the carrier (donor) density, N_D) were corrected for frequency dispersion.

Keywords: Nitinol, passive films, semiconducting properties, electrochemical impedance spectroscopy (EIS), Mott-Schottky analysis (MS)

1. Introduction

Titanium and titanium alloys are commonly used as implant materials for medical and dental application due to their strength, stiffness and toughness, properties important for load bearing applications.[1,2] Nitinol, commercial name for nearly equiatomic alloy of titanium and nickel, exhibits unique properties: superelasticity and shape memory effect in addition to suitable mechanical properties (relatively low elastic modulus, low wear rate, high damping capacity, etc.).[3,4] Due to its desirable properties, Nitinol is widely used for design of state-of-the-art devices in the medical (cardio-vascular stents, guide wires, broken bone staples) and dental field (orthodontic wires and fasteners).[5,6]

Nitinol displays high corrosion resistance in physiological solutions caused by the spontaneously formed biocompatible film of TiO_2.[3,7] The gain in free energy formation, ΔG(298 K) for NiO and TiO_2 is –211.7 and –889.5 kJ mol^{-1}, respectively.[8] However, special attention has been given to its biocompatibility because of the high Ni content. Nickel is an essential element for the human body, but it is allergenic and toxic when present at elevated levels upon dissolving in aggressive bioenvironment of human body leading to infections and compromised implant mechanical integrity.[9,10] Thus, in order to improve its corrosion resistance and prevent the unwanted Ni^{2+} ions release, the modification of Nitinol implant surface is required since other titanium-based alloys used in biomedical applications do not possess its unique properties and thus cannot replace this material.[10–14]

Anodization in acetic acid has been reported to be an effective means of producing and oxide layer on Nitinol, improving its corrosion and biocompatibility properties.[15–20] In our previous papers, the kinetics of the passive oxide film formation and growth on Nitinol in acetic acid was investigated galvanostatically and potentiostatically.[18,20] The experimental results have been explained in the terms of the high field model (HFM) and the point defect model (PDM) that take into account the structure of the growing oxide film.[20–23] The *in situ* growth of the amorphous oxide films on Nitinol under galvanostatic conditions in acetic acid is a high-field assisted process, which proceeds by a cooperative ion conduction mechanism including both metal and oxygen ions migration.[20,24,25] The relevant kinetic parameters for ionic con-

duction in amorphous oxide films on Nitinol were estimated.[20] In the passive crystalline film, formed under potentiostatic conditions, which possesses a certain rigid lattice or sublattice oxide structure, preponderance of anion vacancies over cation vacancies was established according to the PDM diagnostic criteria.[20–23] The flux and diffusivity of oxygen vacancies through the film were calculated using experimentally determined kinetics parameters.[20]

Generally, to predict the long-term corrosion properties of the passivated metals for implant application, it is critical to develop a deep understanding of electronic properties of their surface films. The MS analysis has been very successfully used to study the electronic (semiconducting) properties of passive oxide films on different metal materials, e.g., Fe, Nb, Ni, Cr, stainless steels and titanium.[26–32] However, MS analysis of the capacitance values measured at only one frequency results in loss of or misleading information about characteristic levels of the solid|liquid interface.[26] Thus, it is important to take into account the frequency dispersion, which arises from inhomogeneous current flow,[33,34] and which influences the numerical values of the semiconducting parameters such as the carrier density and the flat-band potential.

In this work, the passive film was formed potentiostatically on Nitinol in acetic acid. After the film stabilization for 24h at the constant potential, the semiconducting properties of passive film were studied by MS analysis under conditions in which its electronic conductivity prevails. Based on the Brug capacitance calculation method[33] and Harrington-Devine method,[35] the MS analysis was performed taking into account the frequency dispersion. The electronic properties were correlated with the results of corrosion investigations performed in simulated physiological Hanks solution.

2. Experimental

The Nitinol foil (NiTi, Alfa Aesar, 55.82 wt.% Ni, ≤0.05 wt.% C, ≤0.05 wt.% O, ≤0.20 wt.% other metal impurities, and balance Ti) was cut into 0.38 mm-thick discs 10 mm in diameter. Circular shaped Nitinol samples were abraded with SiC papers of 240–1200 grit, ultrasonically cleaned with acetone and redistilled water and were used as working electrodes. Electrochemical measurements were performed in a conventional three-electrode cell (volume 500 mL, PAR, Corrosion Cell System, Model K47). The working electrode was embedded in a Teflon holder, with an area of 1 cm^2 exposed to the solution. The counter electrode consisted of two graphite rods and the reference electrode, to which all potentials in the paper are referred, was Ag|AgCl in 3.0 mol dm^{-3} KCl (E = 0.208 V vs. standard hydrogen electrode) connected to the cell via a Luggin probe. A Solartron potentiostat/galvanostat 1287 with FRA 1260 controlled by ZCorr® and ZView® softwares was used in these measurements.

Cyclic voltammogram of the unmodified/bare Nitinol electrode was recorded in an 1 M acetic acid solution (at room temperature, 22±2 °C) in the potential range from –1.5 to +1.5 V with a scan rate of 1 mV s^{-1}. The passive film was formed potentiostatically on Nitinol in acetic acid at the film formation potential, E_f = 0.75 V, where electrode was stabilized for 24 hours.

The electronic-semiconducting properties of the oxide film formed were examined by MS analysis. The capacitance values of the Nitinol|oxide film|solution interface, required for the MS analysis, were determined at selected frequencies from 500–0.5 Hz in an 1 M acetic acid solution (at room temperature, 22±2 °C). The imaginary part of impedance Z_{im} is measured as a function of the electrode potential at a sweep rate of 50 mV s^{-1}, and the interfacial capacitance C is obtained from the relationship $C = -1/\omega Z_{im}$. The rapid cathodic scan of 50 mV s^{-1} was used to avoid the change in the film thickness during the measurements. The potential was swept in the negative direction from film formation potential, E_f = 0.75 V, where electrode was stabilized for 24 hours. Additionally, to find out if the potential scan rate is suitably rapid, MS tests were conducted by scanning the potential in the forward (positive) direction and determining if a hysteresis is present, see Fig. 1. The presence of very slight hysteresis between direct and forward sweep direction at the low frequency of 0.5 Hz indicates that the potential rate is suitably rapid for the MS tests.[35]

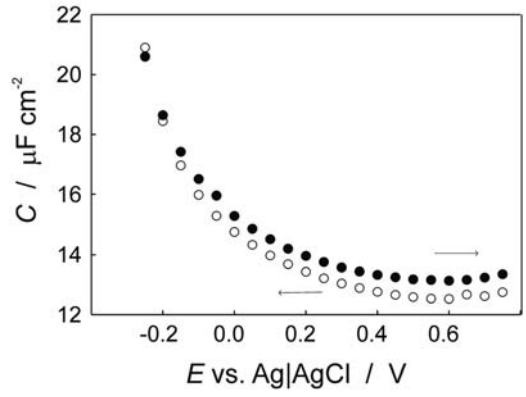

Figure 1. The hysteresis found during the MS scans in the cathodic and anodic directions plotted as a function of the interfacial capacitance, C against the potential applied, E recorded in an acetic acid solution at the constant frequency of 0.5 Hz (sweep directions noted).

The corrosion behavior of Nitinol electrode covered by spontaneously and potentiostatically formed oxide films was studied in Hanks' solution (37 °C) consisting of: 8 g NaCl; 0.4 g KCl, 0.35 g $NaHCO_3$, 0.25 g $NaH_2PO_4 \times H_2O$, 0.06 g $Na_2HPO_4 \times 2H_2O$, 0.19 g $CaCl_2 \times 2H_2O$, 0.19 g $MgCl_2$, 0.06g $MgSO_4 \times 7H_2O$; 1g glucose in 1L of distilled water. EIS measurements were performed in the frequency range from 100 kHz to 5 mHz at an ac voltage

amplitude of 5 mV at the open circuit potential, E_{ocp} after stabilization of 1 hour. The experimental data were fitted using the complex non-linear least squares (CNLS) fit analysis software,[36] and values of the elements of the proposed equivalent circuit were derived with χ^2 values less than 2×10^{-3} (errors in parameter values of 0.5–3%).

3. Results and Discussion

3. 1. Formation and Characterization of the Passive Film on the Nitinol Electrode

Cyclic polarization scan, presented in Fig. 2, was conducted to obtain overview of the electrochemical properties of Nitinol in an 1 M acetic acid solution, pH = 2.7. Two distinct regions were observed, from –0.3 to 0.3 V, and from 0.4 to 1.2 V. These regions were ascribed to the formation of a Ti oxide/hydroxide layer containing different titanium oxides.[20,37] First region corresponds to the formation of titanium suboxides, TiOOH and Ti_2O_3 followed by slight increase in the current density around 0.3 V pointing to the transformation of Ti(III) to Ti(IV) oxides. In the reverse scan, at $E = –0.5$ V hydrogen adsorption and evolution takes place. The anodic part of the cyclic voltammogram indicates that the passivation was completed at 1.4 V. The current increase at $E \geq 1.4$ V is related to the transpassive nickel dissolution and oxygen evolution.[18,20,41] Based on the cyclic voltammetry results, potential of 0.75 V was selected as the film formation potential (24h) for the MS analysis.

Chemical composition of this film was obtained by the analysis of its XPS spectrum.[20] The Ti 2p XPS spectrum was deconvoluted into four component peaks for Ti, TiO, Ti_2O_3 and TiO_2. The intensities of individual component peaks (Ti, Ti_2O_3 and TiO_2) in the Ti $2p_{3/2}$ peak expressed as percentage to the total intensity of the Ti $2p_{3/2}$ were equal to 4.2, 15.3 and 80.5%. The intensity of TiO peak was below 1% and was neglected. Therefore, the spectra were separated into Ti metal, Ti_2O_3 sub-oxide and TiO_2 oxide component peaks. The film formed potentiostatically on Nitinol at 0.75 V consists predominately of TiO_2. The passive film formation at $E_f > 0.75$ V leads to formation of oxide films with higher nickel content.[18,20,38]

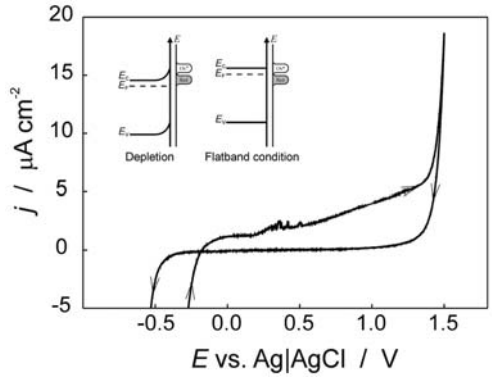

Figure 2. Cyclic voltammogram of the Nitinol electrode recorded in 1 M acetic acid, $\nu = 1$ mV s^{-1}. The insert: The band structure diagrams for n-type semiconductor in contact with an electrolyte under depletion and flat-band conditions.

3. 2. The Semiconducting Properties of the Passive Film on the Nitinol Electrode

After the stabilization of the passive film for 24 hours at $E_f = 0.75$ V, the MS analysis has been used to probe its electronic (semiconducting) properties in an acetic acid solution (pH = 2.7). In MS tests, the interfacial capacitance was measured as a function of both frequency and applied potential in a rapid polarization scan as was described in the Experimental section.

Under depletion conditions at the film|electrolyte interface (see insert in Fig. 2), the MS approximation for n-type semiconductor has the form:[39]

$$1/C_{sc}^2 = \left[2/\left(\varepsilon\varepsilon_0 e N_D\right)\right]\left(E - E_{fb} - kT/e\right) \quad (1)$$

where C_{sc} is the space-charge capacitance, ε_0 is the vacuum permittivity, ε is the dielectric constant of TiO_2 ($\varepsilon = 61$)[40], e is the electron charge, N_D is the donor density, E is the applied potential, E_{fb} is the flat-band potential, k is the Boltzmann constant and T is the temperature. The insert in Fig. 2 is a schematic presentation of the band structure of an n-type semiconductor under flat-band and depletion conditions. Electrons can easily move through an n-type semiconductor below its E_{fb}, while band bending creates a barrier to electron transfer at potentials anodic to E_{fb}.

The electric equivalent circuit (EEC) shown in Fig. 3a represents the impedance of the electrode|electrolyte interface when the electrode is immersed in an aqueous electrolyte solution and covered by a passive film. In this circuit, R_{el} is the electrolyte resistance, R_p is the polarization resistance and C is equal to $(C_{sc}^{-1} + C_H^{-1})$ where C_H is the Helmholtz capacitance. In our case, C is approximately equal to C_{sc} since the C_H for the oxide film|electrolyte solution interface is in order of 100 μF cm^{-2}.[41]

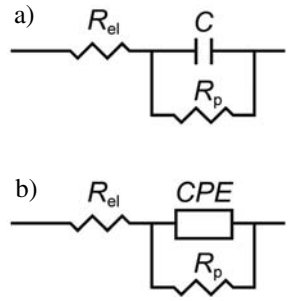

Figure 3. The schematic presentation of the electric equivalent circuits (EECs).

The MS plots for the passive film recorded at constant frequencies noted are presented in Fig. 4. The linear dependence of C_{sc}^{-2} against E with a positive slope is observed suggesting n-type semiconductor behavior. From the values of slopes and intercepts, shown in Fig. 4, using the equation (1), the values of N_D and E_{fb} were calculated (given in Table 1). The calculated E_{fb} values are in good agreement with literature data for oxide films formed on titanium/titanium alloys[29,31,41,42] (E_{fb} values vary with crystallographic structure of the oxide and the nature of the electrode material).[43–45] The obtained values of N_D in the range of 10^{20} cm^{-3} point to formation of highly-doped n-type semiconductor.[31,41,46,47] The donor level is slightly less than those of most passive metals (10^{20}–10^{21} cm^{-3}), such as Ni and Fe,[27,28] but slightly higher than that of bulk rutile (10^{18}–10^{19} cm^{-3}).[48]

The MS plots presented in Fig. 4 and the N_D and E_{fb} values given in Table 1, clearly show the dependence on the frequency used. Therefore, to avoid the frequency dispersion in MS tests, the data obtained at nine frequencies were analyzed according to the procedure proposed by Harrington et al.[35,49] The Z_{im} versus E dependences measured at different frequencies were used to construct a Bode diagram containing a set of log $|Z|$ versus log f at 8 potential values inside the potential region investigated at steps of 50 mV (Fig. 5).

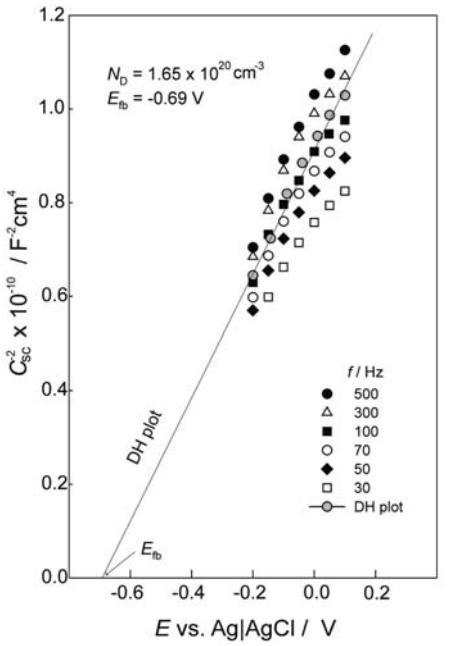

Figure 4. The Mott–Schottky plots of the Nitinol electrode covered by the passive film recorded in an acetic acid solution at the different frequencies noted. The plot obtained by applying Devine and Harrrington procedure is labeled "DH plot".

Table 1. The values of the charge carrier density, N_D and the flat-band potentials, E_{fb} of the passive film formed on the Nitinol electrode in an acetic acid solution.

f / Hz	$N_D \times 10^{-20}$ / cm^{-3}	E_{fb} / V
500	1.52	–0.69
300	1.86	–0.71
100	1.89	–0.75
70	1.83	–0.70
50	1.93	–0.71
30	2.08	–0.70

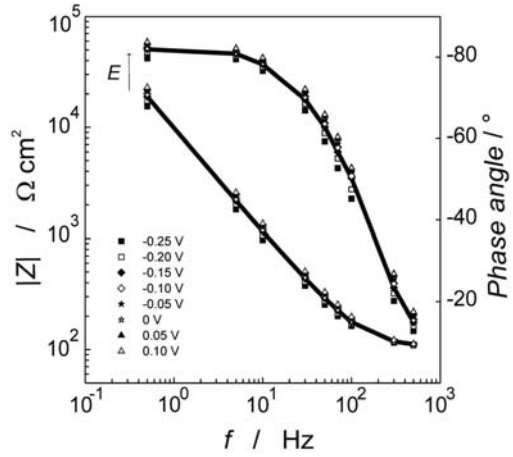

Figure 5. Bode plot constructed from the Mott–Schottky measurements of the Nitinol electrode covered by the passive film recorded in an acetic acid solution at the potentials noted.

Each of these log $|Z|$ versus log f plots was fitted using the complex non-linear least squares (CNLS) fit analysis software ZView®.[36] For the fitting, the modified Randles equivalent circuit was used (Fig. 3b), where a constant-phase element, CPE is used instead of a capacitance.[34] The impedance of CPE is described by an empirical impedance function of the type:

$$Z(\mathrm{CPE}) = [Q(j\omega)^n]^{-1} \quad (2)$$

where Q is the constant of the CPE element, $j\omega$ is the complex variable for sinusoidal perturbations with $\omega = 2\pi f$, and n is the exponent of CPE.[33,34] The use of CPE is necessary to account for the non-ideal capacitance of the electrode. The CPE behavior is thought to be caused by a distribution of time constants due to inhomogeneous current flow.[33,34]

The fitting parameters R_{el}, Q, n, and R obtained at nine frequencies at different potential values (Table 2) were used to calculate the capacitance at each potential value according to the Brug at al.[33]

$$Q = C^n (R_{el}^{-1} + R^{-1})^{1-n} \quad (3)$$

As it was mentioned before, in our case, C is approximately equal to C_{sc}. Thus, the C_{sc}^{-2} versus E dependence

Table 2. Impedance parameters of the Nitinol electrode covered by passive film obtained for Bode plots constructed from the Mott-Schottky measurements at different frequencies in an acetic acid solution.

E/V	$Q \times 10^6$/ Ω^{-1} cm^{-2} s^n	*n*	*R*/ MΩ cm^2	*C*/ μF cm^{-2}
–0.25	22.49	0.925	0.28	13.77
–0.20	19.94	0.929	0.49	12.46
–0.15	18.35	0.932	0.68	11.58
–0.10	17.31	0.933	0.89	11.00
–0.05	16.56	0.934	1.33	10.59
0	15.60	0.935	1.75	10.26
0.05	15.50	0.937	2.64	10.07
0.10	15.15	0.938	3.69	9.86

R_{el} = 103.6 ± 0.3 Ω cm^2

obtained in this way (Table 2) is presented in Fig. 4 (noted: DH plot) and lies between dependences obtained at frequencies 300 and 100 Hz. From the slope of the DH plot, using Eq. (1), the values of $N_D = 1.65 \times 10^{20}$ cm^{-3} and E_{fb} = –0.69 V were obtained and are in good agreement with those reported previously.[20,31,41,42,50]

From the experimentally determined values of N_D and E_{fb}, the value of the thickness of the space-charge layer, d_{sc} was calculated by relation:[51]

$$d_{sc} = [2\varepsilon\varepsilon_0 (E - E_{fb} - kT/e) / (eN_D)]^{1/2} \quad (4)$$

The obtained d_{sc} value of 5.4 nm is smaller than the oxide film thickness obtained in our previous work by XPS measurements (d_{film} = 8.2 nm)[20] confirming the validity of the MS analysis. By comparing the values obtained, it follows that the space-charge layer occupies the great part of the oxide film.

During polarization of the passivated Nitinol electrode in the potential region from –0.25 V to 0.10 V the majority of the charge carriers (electrons) has been removed (transferred from the electrode into solution). Therefore, there is a positive charge of the immobile donors, and this is reflected in an upward band bending of the band edges. The result is an increase of the potential drop within the oxide layer (limited by the conditions $\Delta E < E - E_{fb}$), as well as an increase of the depletion (space charge) layer and the resistance of the oxide film (space charge layer) (Table 2).

3. 3. Corrosion Behavior of Passivated Nitinol in Simulated Body Fluid

The corrosion resistance of passivated Nitinol, as a key factor for implant biocompatibility in contact with body fluids, was investigated in physiological conditions (under *in vitro* conditions of real implant application).

Impedance spectra were recorded on spontaneously and potentiostatically formed oxide films on Nitinol after various periods of immersion in Hanks' solution (Fig. 6). The EIS data were analyzed in terms of the EEC shown in Fig. 3b using the CNLS fit analysis software ZView®.[36] The numerical values for the EIS parameters are listed in Table 3.

The polarization resistance of the barrier layer, inversely proportional to the corrosion rate, is much higher on potentiostatically anodized than on spontaneously anodized Nitinol. The protection effectiveness of the potentiostatically anodized film, η was calculated using the relation:

$$\eta = R_{p,(anod)} - R_{p,(spont)} / R_{p,(anod)} \quad (5)$$

where $R_{p,(anod)}$ and $R_{p,(spont)}$ are the values of R_p in Fig. 6 and Table 3. The protection effectiveness of 95% indicates the excellent corrosion resistance of potentiostatically oxidized Nitinol under *in vitro* conditions.

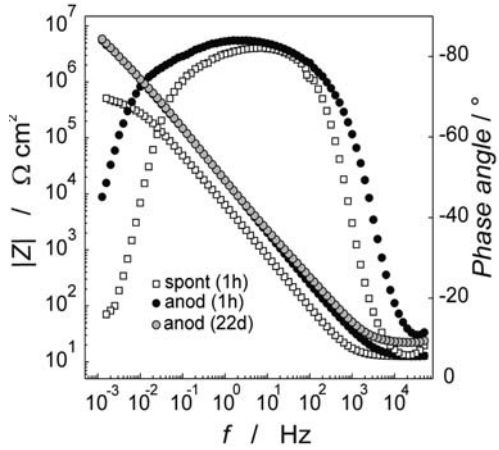

Figure 6. Impedance spectra of the Nitinol electrode covered by spontaneously and potentiostatically formed oxide films recorded in Hanks' solution after various immersion times at open circuit potential.

Table 3. Impedance parameters of the Nitinol electrode covered by spontaneously and potentiostatically formed oxide films recorded in Hank's solution after various immersion times at open circuit potential.

E/V	$Q \times 10^6$/ Ω^{-1} cm^{-2} s^n	*n*	*C*/ μF cm^{-2}	R_p/ MΩ cm^2	η/%
Nitinol covered with spontaneously formed oxide film					
1 h	30.11	0.912	13.82	0.44	/
Nitinol covered with anodically formed oxide film					
1 h	12.87	0.929	6.60	8.02	94.3
1 d	10.89	0.913	4.81	8.86	94.8
6 d	10.43	0.897	3.88	13.87	96.7
22 d	10.52	0.886	3.48	13.28	96.5

R_{el} = 12.5 Ω cm^2

4. Conclusions

Nitinol is widely used in many medical applications: as cardiovascular, dental and orthopedic implant material. In order to enhance this material's corrosion resistance and biocompatibility, the surface of Nitinol was coated with the passive oxide film formed potentiostatically in an acetic acid solution.

The oxide film|electrolyte interface has been treated as space charge depletion zone, which acts as Schottky barrier. The electronic (semiconducting) properties determined from capacitance measurements using Mott-Schottky analysis show that passive film on Nitinol behaves as a highly doped n-type semiconductor. The MS tests were performed suitably rapid that the film did not change during the test (assessed by slight hysteresis between the forward and reverse potential scans). Taking into account the frequency dispersion in MS tests, the semiconducting parameters were determined:

– The donor density, $N_D = 1.65 \times 10^{20}$ cm^{-3}

– The flat-band potential, $E_{fb} = -0.69$ V vs. Ag|AgCl

– The space-charge layer thickness, $d_{sc} = 5.4$ nm.

In situ investigations of corrosion resistance of passivated Nitinol under *in vitro* conditions of real implant material application performed by EIS have shown that passivated Nitinol exhibits a high corrosion resistance. The protection efficiency was 95% demonstrating the resistance against general and localized corrosion of Nitinol in the simulated body fluid containing Cl^- ions. The excellent corrosion stability of passivated Nitinol in physiological conditions was correlated with the n-type semiconducting properties of its passive film.

List of Symbols

C	capacitance (F cm^{-2})
CPE	constant-phase element
C_H	Helmholtz capacitance (F cm^{-2})
C_{sc}	space-charge capacitance (F cm^{-2})
d_{film}	oxide film thickness (nm)
d_{sc}	space-charge layer thickness (nm)
e	electron charge (1.602×10^{-19} C)
E	potential (V)
E_C	conduction band
E_F	Fermi level
E_f	film formation potential (V)
E_{fb}	flat-band potential (V)
E_{OCP}	open circuit potential (V)
E_V	valence band
f	frequency (Hz)
ΔG	free energy formation (J mol^{-1})
j	current density (A cm^{-2})
$j\omega$	complex variable for sinusoidal perturbations with $\omega = 2\pi f$
k	Boltzmann constant (1.38×10^{-23} J K^{-1})
n	CPE power
N_D	donor density (cm^{-3})
R_{el}	electrolyte (ohmic) resistance (Ω cm^2)
R_p	polarization resistance (Ω cm^2)
Q	constant of the CPE element (Ω^{-1} cm^{-2} s^n)
T	temperature (K)
Z	electrode impedance (Ω cm^2)
Z_{im}	imaginary part of impedance (Ω cm^2)
ε	dielectric constant of the surface film
ε_o	dielectric constant of vacuum (8.85×10^{-14} F cm^{-1})
η	protection effectiveness (%)
ν	scan rate (mV s^{-1})
ω	angular frequency (Hz)

5. References

1. B. D. Ratner, A. S. Hoffman, F. J. Schoen, J. E. Lemons (Ed.): Biomaterials Science an Introduction to Materials in Medicine, Elsevier, Academic Press, San Diego, London, **2004**.
2. M. Geetha, A.K. Singh, R. Asokamani. A.K. Gogia, *Prog. Mater. Sci.* **2009**, *54*, 397–425.
3. S. A. Shabalovskaya, *Bio-Med. Mater. Eng.* **2002**, *12*, 69–109.
4. R. Liu, D. Li, *Mater. Sc. Eng. A* **2000**, *277*, 169–175.
5. T. Duerig, A. Pelton, S. Stockel, *Mater. Sci. Eng. A* **1999**, *273–275*, 149–160.
6. N. B. Morgan, *Mater. Sci. Eng. A* **2004**, *378*,16–23.
7. N. Figueira, T. M. Silva, M. J. Carmezin, J. C. S. Fernandes, *Electrochim. Acta* **2009**, *54*, 921–926.
8. S. A. Shabalovskaya, G. C. Rondelli, A. L. Undisz, J. W. Aneregg, T. D. Burleigh, M. E. Rettenmayr, *Biomaterials* **2009**, *30*, 3662–3671.
9. D. Granchi, G. Ciapetti, L. Savarino, S. Stea, F. Filippini, A. Sudanese, R. Rotini, A. Giunti, *Biomaterials* **2000**, *21*, 2059–2065.
10. S. A. Shabalovskaya, J. Anderegg, J. van Humbeeck, *Acta Biomater.* **2008**, *4*, 447–467.
11. Ž. Petrović, J. Katić, M. Metikoš-Huković, H. Dadafarin, S. Omanovic, *J. Electrochem. Soc.* **2011**, *158*, 159–165.
12. J. Katić, M. Metikoš-Huković, R. Babić, M. Marciuš, *Int. J. Electrochem. Sci.* **2013**, *8*, 1394–1408.
13. J. Katić, M. Metikoš-Huković, R. Babić, *J Appl. Elctrohem.* **2014**, *44*, 87–96.
14. J. Katić, M. Metikoš-Huković, S. D. Škapin, M. Petravić, M. Varašanec, *Electrochim. Acta* **2014**, *127*, 173–179.
15. F. T. Cheng, P. Shi, G. K. H. Pang, M. H. Wong, H. C. Man, *J. Alloys Compd.* **2007**, *438*, 238–242.
16. P. Shi, F. T. Cheng, H. C. Man, *Mater. Lett.* **2007**, *61*, 2385–2388.
17. C. L. Chu, R. M. Wang, T. Hu, L. H. Yin, Y. P. Pu, P. H. Lin, Y. S. Dong, C. Guo, C. Y. Chung, K. W. K. Yeung, P. K. Chu, *J. Mater. Sci.: Mater. Med.* **2009**, *20*, 223–228.
18. J. Katić, M. Metikoš-Huković, *ECS Trans.* **2010**, *28*, 65–75.

19. I. Milošev, D. Blejan, S. Varvara, L. M. Muresan, *J. Appl. Electrochem.* **2013**, *43*, 645–658.
20. M. Metikoš-Huković, J. Katić, I. Milošev, *J. Solid State Electrochem.* **2012**, *16*, 2503–2513.
21. M. M. Lohrengel, *Mater. Sci. Eng. R* **1993**, *11*, 243–294.
22. D. D. Macdonald, M. Urquidi-Macdonald, *J. Electrochem. Soc.* **1990**, *137*, 2395–2402.
23. D. D. Macdonald, *J. Electrochem. Soc.* **1992**, *139*, 3434–3449.
24. J. P. S. Pringle, *Electrochim. Acta* **1980**, *25*, 1423–1437.
25. M. H. Wang, K. R. Hebert, *J. Electrochem. Soc.* **1999**, *146*, 3741–3749.
26. F. Di Quarto, F. La Mantia, M. Santamaria, *Electrochim. Acta* **2005**, *50*, 5090–5102.
27. A. J. Ahn, H. S. Kwon, *Electrochim. Acta* **2004**, *49*, 3347–3353.
28. E. Sikora, D. D. Macdonald, *Electrochim. Acta* **2002**, *48*, 69–77.
29. M. Schneider, S. Schroth, J. Schilm, A. Michaelis, *Electrochim. Acta* **2009**, *54*, 2663–2671.
30. Ž. Petrović, N. Lajci, M. Metikoš-Huković, R. Babić, *J. Solid State Electrochem.* **2011**, *15*, 1201–1207.
31. Z. Jiang, X. Dai, H. Middleton, *Mater. Chem. Phys.* **2011**, *126*, 859–865.
32. L. Hamadou, A. Kadri, N. Benbrahim, *Appl. Surf. Sci.* **2005**, *252*, 1510–1519.
33. G. J. Brug, A. L. G. van der Eeden, M. Sluyters-Rehbach, J. H. Sluyters, *J. Electroanal. Chem.* **1984**, *176*, 275–295.
34. J. B. Jorcin, M. E. Orazem, N. Pebere, B. Tribollet, *Electrochim. Acta* **2006**, *51*, 1473–1479.
35. S. P. Harrington, T. M. Devine, *J. Electrochem. Soc.* **2008**, *155*, C381–386.
36. A. Boukamp, *Solid State Ionics* **1986**, *20*, 31–44.
37. M. Metikoš-Huković, A. Kwokal, J. Piljac, *Biomaterials* **2003**, *24*, 3765–3775.
38. L. A. S. Ries, M. Da Cunha Belo, M. G. S. Ferreira, I. L. Muller , *Corr. Sci.* **2008**, *50*, 676–686.
39. S. R. Morrison, Electrochemistry at semiconductor and oxidized metal electrodes, Plenum, New York, **1980,** p. 133**.**
40. J. Marsh, G. Gorse, *Electrochim Acta* **1998**, *43*, 659–670.
41. I. U. Petersson, J. E. L. Löberg, A. S. Fredriksson, E. K. Ahlberg, *Biomaterials* **2009**, *30*, 4471–4479.
42. A. G. Munoz, *Electrochim. Acta* **2007**, *52*, 4167–4176.
43. B. Bozzini, P. Carlino, L. D'Urzo, V. Pepe, C. Mele, F. A.Venturo, *J. Mater. Sci. Mater. Med.* **2008,** *19*, 3443–3453.
44. M. Radecka, M. Rekas, A. Trenczek-Zajac, K. Zakrzewska, *J. Power Sources* **2008**, *181*, 46–55.
45. J. W. Schultze, M. M. Lohrengel, *Electrochim. Acta* **2000**, *45*, 2499–2513.
46. S. K. Poznyak, A. D. Lisenkov, M. G. S. Ferreira, A. I. Kulak, M. L. Zheludkevich, *Electrochim. Acta* **2012**, *76*, 453–461.
47. D. Sazou. K. Saltidou, M. Pagitsas, *Electrochim. Acta* **2012**, *76*, 48–61.
48. T. Bak, J. Nowotny, M. Rekas, C. C. Sorrell, *J. Phys. Chem. Sol.* **2003**, 64, 1057–1067.
49. S. P. Harrington, F. Wang, T. M. Devine, *Electrochim. Acta* **2010**, *55*, 4092–4102.
50. G. Wan, P. Li, X. Xiang, J. Zhou, N. Huang, *J. Mater. Sci.* **2013**, *48*, 4109–4116.
51. R. Memming, in B. E. Conway, J. O'M. Bockris, E. Yeager, S. U. M. Khan, R. E. White (Ed): Comprehensive Treatise of Electrochemistry, Vol. 7, Plenum, New York, **1983,** p. 529.

Povzetek

Oksidno plast (TiO_2) smo tvorili potenciostatski na Nitinolu v ocetni kislini. Da bi lahko napovedali dolgoročno korozijsko vedenje vsadkov, ki so izdelani iz zlitine Nitinola, v simulirani fiziološki raztopini je potrebno podrobno razumevanje elektronskih lastnosti nastale plasti. Meritve kapacitivnosti smo izvedli z namenom študija elektronskih (polprevodnih) lastnosti. Prostorski naboj, ki se tvori na meji trdno|tekoče, predstavlja bariero za korozijski proces v agresivnem biookolju. Glede na rezultate elektrokemijske impedančne spektroskopije in Mott-Schottky analizo se pasivna plast na Nitinolu vede kot amorfni, visokodopirani polprevodnik n-tipa. Pri parameterih elektronske strukture (potencial ravnega pasu, E_{fb} in donorska gostota, N_D) smo upoštevali korekcijo zaradi disperzije frekvencije.